

# Phase Noise of Distributed Oscillators

Xiaofeng Li, O. Ozgur Yildirim, Wenjiang Zhu, and Donhee Ham

**Abstract**—In distributed oscillators, a large or infinite number of voltage and current variables that represent an oscillating electromagnetic wave are perturbed by distributed noise sources to result in phase noise. Here we offer an explicit, physically intuitive analysis of the seemingly complex phase-noise process in distributed oscillators. This study, confirmed by experiments, shows how the phase noise varies with the shape and physical nature of the oscillating electromagnetic wave, providing design insights and physical understanding.

**Index Terms**—Distributed oscillators, oscillators, phase noise, pulse oscillators, soliton oscillators, standing-wave oscillators.

## I. INTRODUCTION

PHASE NOISE is among the most essential and interesting aspects of oscillator's dynamics and quality [1]–[12]. The phase noise of an  $LC$  oscillator [see Fig. 1(a)], where noise perturbs the voltage across, and the current in, the  $LC$  tank, is well understood, owed to works developed until 1960s. For example, Lax's 1967 work [1] provided a tremendous fundamental understanding of phase noise in  $LC$  oscillators.

In contrast, phase-noise processes are harder to grasp in distributed oscillators, or wave-based oscillators, where energy storage components and/or gain elements are distributed along waveguides or transmission lines to propagate electromagnetic waves. The difficulty arises as a large or infinite number of voltage and current variables representing a wave are continually perturbed by noise sources distributed along waveguides or transmission lines. How can we visualize the complex perturbation dynamics and calculate phase noise of distributed oscillators? How does phase noise depend on waveforms, and how can we reconcile it with thermodynamic concepts? An explicit analysis of phase noise in distributed oscillators, which can offer physical understanding, remains to be carried out.

In this paper, we conduct an explicit physically intuitive analysis of phase noise in distributed oscillators. The starting point is our realization that the comprehensive phase-noise framework established in 1989 by Kaertner [2], where he extended Lax's phase-noise study to deal with any general number of

voltage and current variables in oscillators, is applicable to the distributed oscillators. Our explicit application of Kaertner's framework to phase-noise analysis in distributed oscillators provides physical understanding and design insight. The essence of our analysis is experimentally verified.

Our analysis can be applied to distributed oscillators with arbitrary waveforms along waveguides or transmission lines. As demonstrational vehicles, we use three distributed oscillators, shown in Fig. 1(b)–(d). Each oscillator consists of a transmission line, an active circuit at one end of the line, and an open at the other line end. Both the open end and active circuit reflect an oncoming wave so that the wave can travel back and forth on the transmission line. The reflection by the active circuit comes with an *overall* gain, which compensates the line loss. Depending on the specific gain characteristic, different oscillation waveforms result. If the active circuit amplifies small voltages and attenuates large voltages as in standard  $LC$  oscillators, sinusoidal standing waves are formed on the transmission line [13], [14] [see Fig. 1(b)]. If the active circuit attenuates small voltages and amplifies large voltages,<sup>1</sup> a bell-shaped pulse is formed and travels back and forth on the line [15] [see Fig. 1(c)]. If the normal, linear transmission line in Fig. 1(c) is replaced with a nonlinear transmission line, a line periodically loaded with varactors, as in Fig. 1(d), again a pulse is formed [16], [17], but the line nonlinearity sharpens the pulse into what is known as a soliton pulse, which is much sharper than the linear pulse [16]–[20].

Using these oscillators, we show how to calculate phase noise in distributed oscillators, a central outcome of this work. Another main outcome is that the calculation reveals (and experiments confirm) how phase noise of distributed oscillators depends on their waveforms: specifically, it is shown that the linear pulse oscillator [see Fig. 1(c)] has lower phase noise than the sinusoidal standing-wave oscillator [see Fig. 1(b)]. Not only is this result useful from the design point of view, but it offers fundamental physical understanding if reconciled with thermodynamic concepts. In the sinusoidal standing-wave oscillator, one resonating mode is dominantly excited. Just like in the  $LC$  oscillator, the single resonating mode possesses two degrees of freedom, namely, the electric and magnetic fields (voltage and current standing waves), each storing a mean thermal energy of  $kT/2$  ( $k$ : Boltzmann's constant;  $T$ : temperature) according to the equipartition theorem. Overall, a total thermal energy of  $kT$  perturbs the single resonating mode. This thermodynamic notion is in congruence with our analysis; thus, the sinusoidal standing-wave oscillator can be treated like the  $LC$  oscillator without having to resort to our analysis developed for general distributed oscillators. By contrast, in the pulse oscillator, the oscillating pulse contains multiple harmonic modes, thus, the equipartition theorem predicts that the pulse oscillator would

<sup>1</sup>If small voltages are attenuated, oscillation startup cannot occur. A special startup circuit is to be arranged in this case [15]–[17].

Manuscript received October 20, 2009; revised March 07, 2010; accepted April 30, 2010. Date of publication July 19, 2010; date of current version August 13, 2010. This work was supported by the Army Research Office under Grant W911NF-06-1-0290, by the Air Force Office of Scientific Research under Grant FA9550-09-1-0369, and by the World Class University (WCU) Program through the National Research Foundation of Korea funded by the Ministry of Education, Science, and Technology (R31-2008-000-10100-0).

X. Li, O. O. Yildirim, and D. Ham are with the School of Engineering and Applied Sciences, Harvard University, Cambridge, MA 02138 USA (e-mail: xiaofeng@seas.harvard.edu; donhee@seas.harvard.edu).

W. Zhu was with the Department of Chemistry and Chemical Biology, Harvard University, Cambridge, MA 02138 USA. He is now with JP Morgan, New York, NY 10017 USA.

Color versions of one or more of the figures in this paper are available online at <http://ieeexplore.ieee.org>.

Digital Object Identifier 10.1109/TMTT.2010.2053062

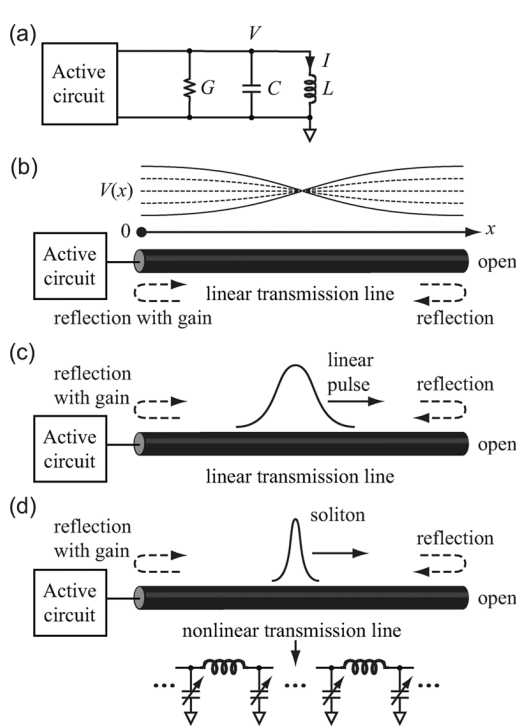


Fig. 1. Oscillator examples. (a)  $LC$  oscillator. (b)  $\lambda/2$  sinusoidal standing-wave oscillator. (c) Linear pulse oscillator. (d) Soliton pulse oscillator.

have higher phase noise than the sinusoidal standing-wave oscillator, which is wrong and opposite the result of our analysis/experiment. The inapplicability of the equipartition theorem in the Fourier domain to the pulse oscillator arises as the multiple harmonic modes are inter-coupled or mode-locked together. The legitimate phase-noise calculation for the pulse oscillator thus calls for a general analysis like ours, which captures the correct physics: noise generated at a given point of a wave propagation medium affects a wave only when it passes through the point, thus, the noise's chance to enter the phase-noise process is smaller for a spatially localized pulse than for a sinusoidal wave spread over the medium. Consequently, the linear pulse oscillator has lower phase noise.

Yet another main outcome of this study involves the soliton pulse oscillator [see Fig. 1(d)]. As the soliton pulse oscillator has a smaller pulsewidth than the linear pulse oscillator [see Fig. 1(c)], according to the foregoing reasoning, the former would have lower phase noise than the latter. However, our analysis shows that this is not necessarily the case: due to the amplitude-dependent propagation speed of solitons, which is a hallmark nonlinear property of solitons, amplitude-to-phase-noise conversion can significantly contribute to phase noise of the soliton oscillator. Not only the waveform, but also the wave's nonlinear nature, plays a role in the phase-noise process in the soliton oscillator.

Our analysis can be readily applied to oscillators with distributed gains [21]. To show the essence simply, however, we do not include them in this paper. The essence is more easily tested with the three example circuits above. In addition, for mathematical simplicity, this paper focuses on phase noise incurred by white noise only, although our analysis can be extended to

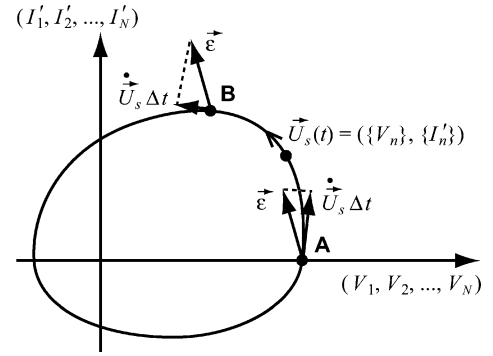


Fig. 2. Oscillator's limit cycle in  $2N$ -D state space. For illustrative purposes, we only show two axes.

deal with  $1/f$  noise sources, as in [3], which is another work by Kaertner, extending his original work [2] to include the effect of  $1/f$  noise.

Section II reviews the fundamental theories of phase noise by Lax [1] and Kaertner [2]. Section III analyzes direct phase perturbations and their effect on phase noise. Section IV examines indirect phase perturbations caused by amplitude-to-phase error conversion, and their effect on phase noise. Sections V and VI present measurements and their analysis.

## II. PHASE-NOISE FUNDAMENTALS: REVIEW OF LAX'S AND KAERTNER'S WORKS

### A. Lax's Fundamental Theory of Phase Noise

The essence of Lax's work [1] may be understood as follows. Consider an  $LC$  oscillator [see Fig. 1(a)]. The voltage  $V$  across and the current  $I$  in the  $LC$  tank represent the oscillator's state. The steady-state oscillation follows a closed-loop trajectory, or limit cycle, in the 2-D  $V$ - $I$  state space (Fig. 2 with  $N = 1$ ). Noise perturbs the oscillation, causing amplitude and phase errors. The amplitude error that puts oscillation *off* the limit cycle is constantly corrected by the oscillator's tendency to return to its limit cycle. In contrast, the phase error *on* the limit cycle along its tangential direction accumulates without bound for no mechanism to reset the phase exists. In other words, the phase undergoes a diffusion along the limit cycle. Due to this *phase diffusion*, the oscillator's output spectrum is broadened around the oscillation frequency, causing phase noise.

Mathematically, in the presence of only white noise, the phase diffusion so occurs that the variance of the phase  $\phi$  of the oscillation  $\cos(\omega_0 t + \phi)$  grows linearly with time

$$\langle \phi^2 \rangle = 2Dt \quad (1)$$

where  $D$  is the phase diffusion rate. This leads to the well-known Lorentzian phase noise

$$\mathcal{L}\{\Delta\omega\} = \frac{2D}{(\Delta\omega)^2 + D^2} \quad (2)$$

and the  $f^{-2}$  behavior for  $\Delta\omega \gg D$

$$\mathcal{L}\{\Delta\omega\} \approx \frac{2D}{(\Delta\omega)^2} \quad (3)$$

which is familiar from Leeson's paper [22].

As seen, once the phase diffusion rate  $D$  is determined, phase noise is known.  $D$  can be determined by evaluating the phase error along the tangential direction of the limit cycle for a given noise perturbation. The phase error depends not only on the noise level, but also on the oscillator state, or the limit cycle position where the perturbation occurs, due to the tangential projection [1]. This state-dependency is illustrated in Fig. 2: the same noise perturbation  $\vec{\varepsilon}$  causes different phase errors at two different limit cycle positions **A** and **B**. Therefore, this state-dependent or time-varying phase error is averaged along the limit cycle, and thus  $D$  will be a function of the oscillator's waveform (limit cycle shape), as well as the noise level [1]. This state-dependent or time-variant property has been greatly exploited by the circuit community for low-noise oscillator design [4].

### B. Kaertner's Generalization

Kaertner expanded Lax's analysis to a general case where an oscillator state is described with  $2N$  variables in a  $2N$ -dimensional ( $2N$ -D) state space (Fig. 2) [2]. Noise perturbations are decomposed into a component along the tangential direction of the oscillator's limit cycle in the  $2N$ -D state space, and components orthogonal to the tangential direction. The former component, as in Lax's work, corresponds to phase perturbation that directly drives the phase diffusion process. Besides, Kaertner considered how the latter components, corresponding to amplitude perturbations, indirectly contribute to phase diffusion through amplitude-to-phase-noise conversion determined by the oscillator's dynamics. This calculation, like Lax's theory, would follow the limit cycle and average the state-dependent phase errors in determining  $D$ . Therefore, it holds true even in the general case treated by Kaertner that  $D$  depends not only on the noise level, but also on the waveform or the shape of the limit cycle: this waveform dependency is a general hallmark property of oscillator's phase diffusion.

The general framework by Kaertner, including the orthogonal projection, is the basis of this work. We translate Kaertner's mathematical language to what can be directly applied to calculating the phase noise of distributed oscillators. We decompose noise perturbations into phase and amplitude perturbations, and study their contributions to phase noise separately in Sections III and IV.

## III. PHASE NOISE DUE TO DIRECT PHASE PERTURBATION

This section calculates the phase diffusion driven directly by the tangential projections of noise perturbations. We use the three transmission-line oscillators in Fig. 1(b)–(d) as demonstrational vehicles.

Before going into detail, let us first visualize the phase-noise process in the transmission-line oscillator's state space. The transmission line can be an artificial medium consisting of  $N$   $LC$  sections (Fig. 3). The corresponding oscillator has  $2N$  state variables, each corresponding to a voltage or current variable of a capacitor or inductor. These  $2N$  variables are collectively represented by a single point  $\vec{U} = (\{V_n\}, \{I_n\})$

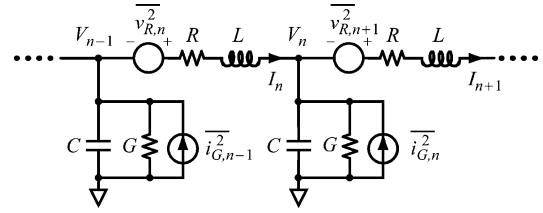


Fig. 3. Artificial transmission line consisting of  $N$   $LC$  sections.  $n = 1, 2, \dots, N$ . Loss components  $R$  and  $G$  are included with associate noise.

( $n = 1, 2, \dots, N$ ) in the  $2N$ -D state space.<sup>2</sup> In the steady state, the state point evolves along a limit cycle,  $\vec{U}_s(t)$  in the  $2N$ -D space (Fig. 2). The  $2N$  voltage and current variables of  $\vec{U}$  are perturbed by noise sources located along the transmission line, and these  $2N$  perturbations can be collectively represented by a single perturbation vector  $\vec{\varepsilon}$  in the  $2N$ -D state space (Fig. 2). Overall, we have a single noise perturbation vector that collectively disturbs a single oscillator state point  $\vec{U}$ , the collection of voltage and current variables, which evolve all together along the limit cycle in the  $2N$ -D state space. Therefore, all voltage and current variables share exactly the same phase diffusion rate, and thus, the same phase noise. Our task is to calculate this common phase diffusion rate.

When the transmission line is a continuous medium (e.g., coplanar stripline), the oscillator possesses infinitely many state variables. This can be dealt with as an extreme case of the artificial line with  $2N \rightarrow \infty$ .

Noise can be distributed along the line (e.g., thermal noise associated with the distributed loss in the line) or lumped (e.g., noise from the lumped active circuit). We will treat these two noise sources separately in Sections III-A and B.

### A. Direct Phase Perturbation Due to Distributed Noise

We first consider the distributed noise from an artificial transmission line with  $2N$  state variables (Fig. 3). The calculation of the direct phase perturbation by the distributed noise runs in two steps. First, by analyzing the oscillator dynamics in the presence of the noise, we identify the vector  $\vec{\varepsilon}$  representing the noise perturbation in the  $2N$ -D state space. Second, we project this noise perturbation vector onto the tangential direction of the limit cycle to calculate the phase error.

To identify the vector of noise perturbation in the  $2N$ -D state space, we apply Kirchhoff's law in Fig. 3<sup>3</sup>

$$C\dot{V}_n = I_n - I_{n+1} - V_n G + i_{G,n}(t) \quad (4a)$$

$$L\dot{I}_n = V_{n-1} - V_n - I_n R + v_{R,n}(t) \quad (4b)$$

where  $n = 1, 2, \dots, N$  and the dot above a variable represents a time derivative. Resistance  $R$  and conductance  $G$  represent loss in the line. Their associated Nyquist voltage and current thermal noise  $v_{R,n}$  and  $i_{G,n}$  satisfy  $\overline{v_{R,n}^2}/\Delta f = 4kTR$  and  $\overline{i_{G,n}^2}/\Delta f = 4kTG$ . Other distributed noise sources, such as

<sup>2</sup>It is assumed that the oscillator's active circuit is memoryless compared to the transmission line, not generating extra state variables.

<sup>3</sup>In case of the nonlinear transmission line, where  $C$  is voltage dependent, the nominal  $C$ -value is used in the following calculations for approximation.

those from distributed gain elements [21], if any, can be similarly modeled.

Change of variables,  $I'_n \equiv I_n Z_0$ ,  $R' \equiv R/Z_0$ , and  $G' \equiv GZ_0$  with an impedance-unit parameter  $Z_0 \equiv \sqrt{L/C}$  renders  $R'$  and  $G'$  dimensionless, and  $I'_n$  with the dimension of voltage. With the new variables, we rewrite (4) into

$$dV_n = [(I'_n - I'_{n+1} - V_n G')dt + \varepsilon_{G,n}]/\sqrt{LC} \quad (5a)$$

$$dI'_n = [(V_{n-1} - V_n - I'_n R')dt + \varepsilon_{R,n}]/\sqrt{LC} \quad (5b)$$

where  $\varepsilon_{R,n} \equiv v_{R,n}(t)dt$  and  $\varepsilon_{G,n} \equiv Z_0 i_{G,n}(t)dt$  are rescaled noise terms that are independent Gaussian random variables with zero mean and variance  $\langle \varepsilon_{R,n}^2 \rangle = 2kTR'Z_0 dt$ ,  $\langle \varepsilon_{G,n}^2 \rangle = 2kTG'Z_0 dt$  [23]. Equation (5) identifies a random vector  $\vec{\varepsilon} = (\{\varepsilon_{G,n}\}, \{\varepsilon_{R,n}\})/\sqrt{LC}$  as the noise perturbation vector during the time interval  $[t, t + dt]$ . Also note that (5) treats voltage and current variables symmetrically, or, in the equal unit, thanks to the change of variable,  $I'_n \equiv I_n Z_0$ .

Now resorting to Kaertner's scheme [2], we project  $\vec{\varepsilon}$  onto the tangential direction of the limit cycle, or the direction of motion in the state space, which is defined by the state-space velocity  $\dot{\vec{U}}_s$  (Fig. 2). The inner product between  $\vec{\varepsilon}$  and the unit vector  $\vec{U}_s/|\dot{\vec{U}}_s|$  is the perturbation along the direction of motion. Division of this tangential perturbation by the magnitude of the velocity  $|\dot{\vec{U}}_s|$  yields the timing error  $\Delta t$ , which is converted to the phase error  $\phi$  using  $\phi = \omega_0 \Delta t$ , where  $\omega_0$  is the oscillation frequency.<sup>4</sup> In sum,

$$\phi = \omega_0 \frac{\vec{\varepsilon} \cdot \dot{\vec{U}}_s}{|\dot{\vec{U}}_s|^2} = \frac{\omega_0}{\sqrt{LC}} \frac{\sum_n \varepsilon_{G,n} \dot{V}_n + \sum_n \varepsilon_{R,n} \dot{I}'_n}{\sum_n \dot{V}_n^2 + \sum_n \dot{I}'_n{}^2}. \quad (6)$$

As stated earlier, Kaertner derived a more general expression for the phase error using the tangential projection [2], and (6) is an explicit reduction of Kaertner's expression, suitable for the distributed oscillators. Since  $\varepsilon_{R,n}$  and  $\varepsilon_{G,n}$  are independent Gaussian random variables with zero mean,  $\phi$  is also Gaussian with zero mean, and its variance is given by

$$\langle \phi^2 \rangle = 2 \times \frac{kTZ_0\omega_0^2}{LC} \frac{G' \sum_n \dot{V}_n^2 + R' \sum_n \dot{I}'_n{}^2}{\left[ \sum_n \dot{V}_n^2 + \sum_n \dot{I}'_n{}^2 \right]^2} \times dt. \quad (7)$$

Since the phase error must accumulate, growing its variance linearly with time, (7) can be directly compared with the phase diffusion model (1) to find the phase diffusion rate  $D$

$$D(t) = \frac{kTZ_0\omega_0^2}{LC} \frac{G' \sum_n \dot{V}_n^2 + R' \sum_n \dot{I}'_n{}^2}{\left[ \sum_n \dot{V}_n^2 + \sum_n \dot{I}'_n{}^2 \right]^2}. \quad (8)$$

Since  $V_n$  and  $I_n$  are periodic functions of time,  $D(t)$  above is an instantaneous rate at a given time, and it varies periodically with time. This is because the size of the phase error even for a fixed noise vector  $\vec{\varepsilon}$  depends on the state of oscillation (where the state lies on the limit cycle), as indicated by (6), as illustrated in Fig. 2, and as mentioned as a hallmark property of the oscillator phase diffusion [1], [2] in Section II. The periodically

<sup>4</sup>The detailed projection procedure up to this part of the present paragraph is generally captured in (16) and (23b) in Kaertner's paper [2].

varying diffusion rate is usually time averaged over one oscillation period to yield a constant diffusion rate, which matters over a long run

$$D = \frac{kTZ_0\omega_0^2}{LC} \left\langle \frac{G' \sum_n \dot{V}_n^2 + R' \sum_n \dot{I}'_n{}^2}{\left[ \sum_n \dot{V}_n^2 + \sum_n \dot{I}'_n{}^2 \right]^2} \right\rangle \quad (9)$$

where  $\langle \cdot \rangle$  represents the time average. This concludes our calculation of the direct phase perturbation and the resulting phase diffusion rate, arising from the distributed noise in the artificial transmission line.

In the case of a continuous transmission line where  $2N \rightarrow \infty$  with infinitesimally small  $LC$  sections, the phase diffusion rate can be directly obtained from (9) by replacing the summations with integrals ( $\sum_n \rightarrow (\Delta x)^{-1} \int dx$ ) and replacing  $L$ ,  $C$ ,  $R'$  and  $G'$  with their values per unit length,  $l$ ,  $c$ ,  $r'$ , and  $g'$  ( $L, C, R', G' \rightarrow l\Delta x, c\Delta x, r'\Delta x, g'\Delta x$ )

$$D = kTZ_0v^2\omega_0^2 \left\langle \frac{g' \int (\partial_t V)^2 dx + r' \int (\partial_t I')^2 dx}{\left[ \int (\partial_t V)^2 dx + \int (\partial_t I')^2 dx \right]^2} \right\rangle \quad (10)$$

where  $x$  is the spatial coordinate along the line,  $\partial_t$  is the partial time derivative, and  $v = 1/\sqrt{LC}$  is the wave velocity on the line (not to be confused with the state-space velocity  $\dot{\vec{U}}_s$ ).

Note that the time-averaged terms in (9) and (10) depend on the shape of the limit cycle or the oscillating waveform, which originates from the state dependency of the phase error [1], [2]. Therefore, distributed oscillators with differing oscillating waveforms will exhibit different phase noise. To see this concretely and to interpret the waveform dependency in thermodynamic terms, we now apply (9) or (10) to the three transmission-line oscillators [see Fig. 1(b)–(d)], but we start with a lumped  $LC$  oscillator.

1) *Lumped LC oscillator*, Fig. 1(a): The voltage and current in the  $LC$  tank of an almost sinusoidal oscillator are given by  $V(t) = A \cos \omega_0 t$  and  $I'(t) = A \sin \omega_0 t$ . Plugging these into (9) with  $N = 1$ , while only taking into account  $G$  with  $R = 0$  to model a parallel loss in the tank, we obtain

$$D_{LC} = \frac{1}{4} \frac{kT \omega_0}{E_s Q} \quad (11)$$

where  $E_s = CA^2/2$  is the total oscillation energy stored in the tank and  $Q = \omega_0 C/G$  is the tank's quality factor. This agrees with Lax's work [1], and can be directly converted to the well-known Leeson's formula [22]. Note that  $kT$  is the total thermal energy in the tank (corresponding to noise) because  $L$  and  $C$  each stores a mean thermal energy of  $kT/2$  according to the equipartition theorem. The ratio of the thermal energy to the oscillation energy  $E_s$  is the noise-to-signal ratio.

2) *Sinusoidal standing-wave oscillator*, Fig. 1(b): Voltage and current standing waves in a continuous transmission line are  $V(x, t) = A \cos \beta x \cos \omega_0 t$  and  $I'(x, t) = A \sin \beta x \sin \omega_0 t$  where  $\beta = \omega_0/v$  is the wavenumber. Plugging these into (10) and performing the integrals over the line length  $d$ , we find

$$D_{\text{sin}} = \frac{kTZ_0v^2}{A^2 d} (r' + g') = \frac{1}{4} \frac{kT \omega_0}{E_s Q} \quad (12)$$

where  $E_s = cdA^2/4$  is the total energy stored in the transmission line, and  $Q = \omega_0/(r/l + g/c)$  is the quality factor of the line. Note that the phase diffusion rate of the sinusoidal standing-wave oscillator above conforms to that of the lumped  $LC$  oscillator in (11). This is expected and can be understood in the Fourier domain: although the distributed voltage and current variables in the transmission line correspond to a large (or infinite) number of degrees of freedom in general, in the sinusoidal standing-wave oscillator, only one resonance mode of the transmission line is effectively excited. Like an  $LC$  tank, this resonance mode possesses only two degrees of freedom, namely, the electric and magnetic fields (voltage and current standing waves), each storing a mean thermal energy of  $kT/2$ . It is then possible to treat sinusoidal standing-wave oscillators effectively as lumped  $LC$  oscillators. In fact, using the Fourier amplitudes as state variables, the dynamical equations of standing-wave oscillators can be reduced to those of lumped  $LC$  oscillators. Such reduction was already carried out in the early stage of the phase-noise study for masers and lasers, whose microwave/optical cavities are indeed distributed waveguides that support microwave/optical standing waves [24]. The foregoing discussion may lead the reader to doubting the usefulness of our analysis. However, as we will show right below that this thermodynamic argument in the Fourier domain fails in the case of pulse oscillators, and our analysis becomes necessary.

- 3) *Linear and soliton pulse oscillators*, Fig. 1(c) and (d): The bell-shaped pulse in both linear and soliton pulse oscillators may be described by the same functional form  $V = A \operatorname{sech}^2[B(x - vt)] \approx I'$  with a full spatial width at half maximum  $W \approx 1.76/B$ , although the soliton pulse tends to be sharper (larger  $B$ ). Therefore, their phase diffusion rates can be calculated together using (10). Since the pulse typically spans a length much shorter than the total length of the line, we can replace the integrals over the line length  $d$  in (10) with integrals over the entire  $x$ -axis,<sup>5</sup> i.e.,

$$\int_0^d (\partial_t V)^2 dx \approx \int_{-\infty}^{\infty} (\partial_t V)^2 dx \quad (13)$$

to obtain

$$D_{\text{pulse}} \approx \frac{kTZ_0\omega_0^2W}{7.5A^2}(r' + g') \approx \frac{W^2}{d^2} \frac{kT}{E_s} \frac{\omega_0}{Q} \quad (14)$$

where  $E_s \approx 0.76cWA^2$  is the total energy carried by the pulse. Equation (14) shows that phase noise of the pulse oscillator improves as the pulse gets sharper, a clear manifestation of the waveform dependency of  $D$  captured by the shape factor (time-averaged term) in (10). This can be physically understood in time domain: noise perturbation generated at position  $x$  affects the oscillator's phase or the timing of the pulse only when the pulse passes through the point. Its chance to enter the phase-noise process thus becomes smaller as the pulsewidth decreases, yielding lower

$D$  and better phase noise. Since  $M = d/W$  is approximately the number of excited harmonic modes that constitute the pulse, (14) may be expressed as  $D \sim (1/M^2) \times (kT/E_s) \times (\omega_0/Q)$ . Had we treated the problem in the Fourier domain assuming that the modes were independent of one another, each mode would store a thermal energy of  $kT$  according to the equipartition theorem, and  $D \sim M \times (kT/E_s) \times (\omega_0/Q)$  would result. This, however, is an incorrect result, larger than the true  $D$  value above by a factor of  $M^3$ . The Fourier domain analysis fails because the harmonic modes are not independent, as their relative phases are coupled (or mode-locked) together. This consideration reveals the usefulness and necessity of our analysis in dealing with pulse oscillators.

Now let us compare the phase diffusion rate of the sinusoidal standing-wave oscillator, (12), and that of the pulse oscillator, (14). Their evident difference is again the indication of the waveform dependency of  $D$ . If the standing-wave oscillator and pulse oscillator have the same amplitude for the same noise level, we have

$$\frac{D_{\text{pulse}}}{D_{\text{sin}}} \approx 1.3 \frac{W}{d}. \quad (15)$$

If the two oscillators have the same power dissipation for the same noise level, we have

$$\frac{D_{\text{pulse}}}{D_{\text{sin}}} \approx \frac{4W^2}{d^2}. \quad (16)$$

Therefore, for a very sharp pulse, ( $W \ll d$ ),  $D_{\text{pulse}} \ll D_{\text{sin}}$ . This physically makes sense as explained above, i.e., noise at any given point on the transmission line has less chance to participate in the phase-noise process for a spatially localized pulse than for a standing wave spread over the transmission line, thus, the pulse oscillator is to have lower phase noise than the sinusoidal standing-wave oscillator. Also we note once again that the Fourier domain argument using the equipartition theorem would predict an opposite and wrong result, i.e., higher phase noise for the pulse oscillator that has a larger number of harmonic modes than the sinusoidal standing-wave oscillator. Since the harmonic modes in the pulse oscillator are inter-coupled, the equipartition theorem cannot be applied to the pulse oscillator, as discussed above.

### B. Direct Phase Perturbation Due to Lumped Noise

The direct phase perturbation by the lumped noise from the active circuit in Fig. 1(b)–(d) can be calculated in a similar fashion. At the output of the active circuit (Fig. 4), Kirchhoff's law gives

$$C\dot{V}_1 = I_a - I_1 + i_a(t) \quad (17)$$

where  $I_a = f(V_1)$  describes the characteristics of the active circuit. Its associated noise source is lumped into  $i_a(t)$  and assumed to be white Gaussian with autocorrelation  $\langle i_a(t_1)i_a(t_2) \rangle = 2kTG_a(t_1)\delta(t_1 - t_2)$ . The noise level, represented by the equivalent output noise conductance  $G_a(t)$ , is generally a function of time, which varies periodically with the oscillation [4].

<sup>5</sup>When the pulse reflects at the line ends, the instantaneous phase diffusion rate  $D(t)$  can be slightly modified due to superposition of the incident and reflected pulses. The result after time averaging, however, remains unaltered.

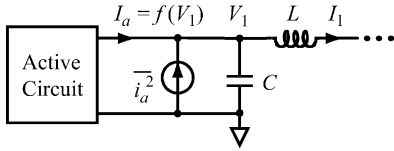


Fig. 4. Circuit model for the active circuit with lumped noise.

As in Section III-A, using change of variables  $I'_n = Z_0 I_n$  and  $G'_a = Z_0 G_a$ , we rewrite (14) into

$$dV_1 = [(I'_a - I'_1)dt + \varepsilon_a]/\sqrt{LC} \quad (18)$$

where  $\varepsilon_a \equiv Z_0 i_a(t)dt$  is a Gaussian random variable with zero mean and variance  $\langle \varepsilon_a^2 \rangle = 2kT Z_0 G'_a dt$ . This equation identifies  $\vec{\varepsilon} = (\varepsilon_a/\sqrt{LC}, 0, \dots, 0)$  as a noise perturbation vector in the  $2N$ -D state space. By projecting  $\vec{\varepsilon}$  along the tangential direction of the limit cycle and following the same procedure in Section III-A, we obtain the following phase diffusion rate due to the direct phase perturbation by the lumped noise for the artificial transmission line case:

$$D = \frac{kT Z_0 \omega_0^2}{LC} \left\langle \frac{G'_a(t) \dot{V}_1^2(t)}{[\sum_n \dot{V}_n^2 + \sum_n \dot{I}_n^2]^2} \right\rangle. \quad (19)$$

In the case of continuous transmission line, it becomes

$$D = kT Z_0 v^2 \omega_0^2 \left\langle \frac{G'_a(t) \dot{V}^2(0, t)}{[\int (\partial_t V)^2 dx + \int (\partial_t I')^2 dx]^2} \right\rangle. \quad (20)$$

The time-averaged terms in (19) and (20) once again exhibit the waveform dependency, as a consequence of the state dependency of the phase error. We again apply these results to the distributed oscillators in Fig. 1(b)–(d). Evaluation of (19) and (20) requires knowledge of the specific form of the time-varying noise level  $G'_a(t)$ . In each of our experimental circuits corresponding to Fig. 1(b)–(d),  $G'_a(t)$  is almost a constant (Section V). Therefore, a constant  $G'_a$  is used in the following calculations.

1) *Sinusoidal standing-wave oscillator*, Fig. 1(b):

$$V(x, t) = A \cos \beta x \cos \omega_0 t \quad \text{and} \quad I'(x, t) = A \sin \beta x \sin \omega_0 t \quad \text{in (20) yield}$$

$$D_{\text{sin}} = \frac{2kT Z_0 G'_a \omega_0^2}{\pi^2 A^2}. \quad (21)$$

2) *Linear and soliton pulse oscillators*, Fig. 1(c) and (d):

At the active circuit end of the line, an incident pulse is superposed with a reflected pulse. The joint voltage amplitude is about twice the incident pulse amplitude, or  $V(0, t) \approx 2A \text{sech}^2(Bvt)$ , assuming linear superposition.<sup>6</sup> Using this and (13) in (20), we obtain

$$D_{\text{pulse}} \approx \frac{kT Z_0 G'_a \omega_0^2 W}{3.76 A^2 d}. \quad (22)$$

<sup>6</sup>In the soliton oscillator case,  $V(0, t)$  may slightly differ from the linear superposition due to the nonlinear interaction between the oncoming and reflected pulses, but we do not expect this to significantly change the result.

Comparing (21) with (22), we find

$$\frac{D_{\text{pulse}}}{D_{\text{sin}}} \approx 1.3 \frac{W}{d} \quad (23)$$

if the standing-wave and pulse oscillators have the same amplitude for the same lumped noise level, and

$$\frac{D_{\text{pulse}}}{D_{\text{sin}}} \approx \frac{4W^2}{d^2} \quad (24)$$

if they have the same power dissipation for the same lumped noise level. These results are exactly the same as in the case of distributed noise perturbation: (15) and (16). The results again indicate that a sharper pulse experiences the lumped noise at  $x = 0$  for a shorter period of time, thus yielding a slower phase diffusion.

We point out that even in the foregoing case of lumped noise, the analysis has still dealt with the distributed nature: the large set of voltage and current variables representing the oscillating electromagnetic wave are distributed along the transmission line, even if the noise source is lumped. The analysis has shown how a perturbation even at one fixed point affects the *collective* oscillation of the entire distributed system.

Thus far we have considered only the direct phase perturbations along the tangential directions of the limit cycle, while not addressing the effect of the amplitude perturbation. As shown by Kaertner, the amplitude perturbation can contribute substantially to phase diffusion through amplitude-to-phase-noise conversion in certain oscillators [2]. This effect is not of great importance in the standing-wave and linear pulse oscillators for the oscillation frequency of the linear transmission line with reasonably high<sup>7</sup>  $Q$  is essentially independent of oscillation amplitude. Therefore, the analysis above is sufficient for the standing-wave and linear pulse oscillators, and it remains valid that the latter has less phase noise than the former. In contrast, in the soliton pulse oscillator, the amplitude perturbation will translate to timing perturbations through soliton's amplitude-dependent propagation speed in the nonlinear transmission line, which can contribute significantly to phase noise. We now turn to this issue for the soliton oscillator.

#### IV. AMPLITUDE PERTURBATION AND ITS PHASE-NOISE EFFECT IN SOLITON OSCILLATORS

This section examines how amplitude perturbation contributes to phase noise in the soliton oscillator through amplitude-to-phase error conversion. We again use Kaertner's orthogonal projection scheme, but we do not carry it out in full to determine the exact amplitude-to-phase error conversion, which requires diagonalizing large matrices corresponding to oscillator's dynamical equations linearized in proximity of its limit cycle. Instead, we evaluate the effect by devising an intuitive phenomenological approach that captures the essence of amplitude-to-phase error conversion in the soliton oscillator.

A soliton pulse propagating in a nonlinear transmission line can be described as  $V = A \text{sech}^2[B(A)(x - v(A)t)] \approx I'$ ,

<sup>7</sup>As seen in Section VI, measured  $Q$  is about 100.

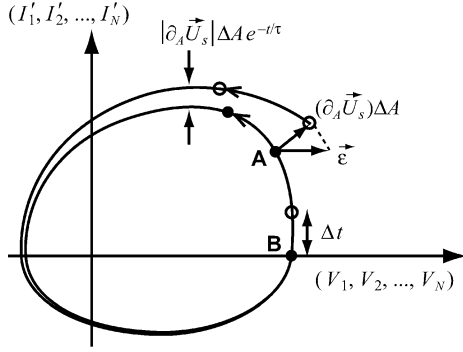


Fig. 5. Amplitude perturbation in the  $2N$ -D state space. Amplitude error  $\Delta A$  is translated to timing error  $\Delta t$  due to the amplitude-dependent speed.

where both the spatial pulsewidth  $W \approx 1.763/B$  and wave velocity  $v$  depend on the amplitude  $A$ . In general, a taller soliton has a narrower width and propagates faster. The exact dependency is determined by the specific form of the line's nonlinearity or the capacitance–voltage relation of the varactors. One particularly well-known example is provided in Appendix [25]. With the pulse waveform above, the limit cycle  $\vec{U}_s$  is now parameterized not only in terms of time  $t$ , but also in terms of amplitude  $A$ .<sup>8</sup> Just like  $\partial_t \vec{U}_s$  giving the direction of phase/timing perturbation,  $\partial_A \vec{U}_s$  defines the direction of amplitude perturbation in the state space. Following a procedure similar to that in Section III, we now calculate the amplitude error by projecting a noise perturbation vector along the direction defined by  $\partial_A \vec{U}_s$  (Fig. 5).

#### A. Indirect Phase Perturbation Due to Distributed Noise

For distributed noise,  $\vec{\epsilon} = (\{\varepsilon_{G,n}\}, \{\varepsilon_{R,n}\})/\sqrt{LC}$  in Section III-A acts again as the noise perturbation vector. It yields the following amplitude error:

$$\begin{aligned} \Delta A &= \frac{\vec{\epsilon} \cdot \partial_A \vec{U}_s}{|\partial_A \vec{U}_s|^2} \\ &= \frac{\sum_n \varepsilon_{G,n} (\partial_A V_n) + \sum_n \varepsilon_{R,n} (\partial_A I'_n)}{\sqrt{LC} [\sum_n (\partial_A V_n)^2 + \sum_n (\partial_A I'_n)^2]}. \end{aligned} \quad (25)$$

$\Delta A$  is Gaussian with zero mean and variance

$$\langle (\Delta A)^2 \rangle = \frac{2kTZ_0}{LC} \frac{\sum_n G'(\partial_A V_n)^2 + R'(\partial_A I'_n)^2}{[\sum_n (\partial_A V_n)^2 + \sum_n (\partial_A I'_n)^2]} dt. \quad (26)$$

Unlike phase perturbation, the amplitude perturbation puts the oscillation off the limit cycle and is corrected in finite time by the oscillator's dynamics. Thus, the amplitude error cannot accumulate indefinitely, but decays exponentially as  $\Delta A e^{-t/\tau}$  (Fig. 5) where  $\Delta A$  is the initial amplitude error and  $\tau$  is the lifetime of the decay, which is determined by the oscillator's loss and gain characteristics. Since the soliton propagation velocity

<sup>8</sup>A similar parametrization of the limit cycle was used by Haus [26] in his study of the noise processes in soliton lasers.

$v$  is a function of  $A$ , this decaying amplitude perturbation will incur a velocity variation of  $\Delta v$  according to

$$\Delta v = \frac{\partial v}{\partial A} \Delta A e^{-t/\tau}$$

which will translate to a total position shift of

$$\Delta x = \int_0^\infty \Delta v dt = \int_0^\infty \frac{\partial v}{\partial A} \Delta A e^{-t/\tau} dt = \frac{\partial v}{\partial A} \Delta A \tau.$$

This is equivalent to a timing error of

$$\Delta t = \frac{\Delta x}{v} = \frac{\tau}{v} \frac{\partial v}{\partial A} \Delta A.$$

Therefore, the total contribution to the timing uncertainty by  $\Delta A$  generated during  $[t, t + dt]$  is

$$\langle (\Delta t)^2 \rangle = \left( \frac{\partial v}{\partial A} \frac{\tau}{v} \right)^2 \langle (\Delta A)^2 \rangle. \quad (27)$$

Plugging (26) into (27) and comparing the result with (1), we find the phase diffusion rate  $D$  due to the amplitude perturbation to be

$$\begin{aligned} D &= \left( \frac{\partial v}{\partial A} \frac{\tau \omega_0}{v} \right)^2 \frac{kTZ_0}{LC} \\ &\quad \times \left\langle \frac{\sum_n G'(\partial_A V_n)^2 + R'(\partial_A I'_n)^2}{[\sum_n (\partial_A V_n)^2 + \sum_n (\partial_A I'_n)^2]} \right\rangle. \end{aligned} \quad (28)$$

In continuous coordinate, this becomes

$$D = \left( \frac{\partial v}{\partial A} \tau \omega_0 \right)^2 kTZ_0 \left\langle \frac{\int g'(\partial_A V)^2 + r'(\partial_A I')^2 dx}{[\int (\partial_A V)^2 + (\partial_A I')^2 dx]^2} \right\rangle. \quad (29)$$

The phase diffusion rate depends on: 1) the sensitivity of amplitude to noise perturbations, captured by  $\int (\partial_A V_n)^2 dx$  and  $\int (\partial_A I'_n)^2 dx$ ; 2) the sensitivity of velocity to amplitude ( $\partial v/\partial A$ ); and 3) lifetime  $\tau$ , i.e., how fast the amplitude error is corrected by the oscillator.<sup>9</sup>

#### B. Indirect Phase Perturbation Due to Lumped Noise

Similar results can be obtained for the lumped noise source described in Section III-B

$$D = \left( \frac{\partial v}{\partial A} \frac{\tau \omega_0}{v} \right)^2 \frac{kTZ_0}{LC} \left\langle \frac{G'_a(t) [\partial_A V_1(t)]^2}{[\sum_n (\partial_A V_n)^2 + \sum_n (\partial_A I'_n)^2]} \right\rangle \quad (30)$$

for an artificial nonlinear transmission line, and

$$D = \left( \frac{\partial v}{\partial A} \tau \omega_0 \right)^2 kTZ_0 \left\langle \frac{G'_a(t) [\partial_A V(0, t)]^2}{[\int (\partial_A V)^2 + (\partial_A I')^2 dx]^2} \right\rangle \quad (31)$$

for a nonlinear line approaching the continuous limit.

<sup>9</sup>In [2], the decay behavior of amplitude error and its translation to phase error are generally captured in (20) and the first term of (26).

### C. Indirect Versus Direct Phase Perturbations

Let us first note that the total phase diffusion rate in a soliton oscillator is a sum of  $D_t$  caused by direct phase perturbations and  $D_A$  induced by amplitude perturbations. This simple addition is possible because the amplitude perturbation [e.g., (25)] and the phase perturbation [e.g., (6)] are orthogonal or uncorrelated to each other. This orthogonality can be checked by noticing that  $\partial_A V$  and  $\partial_A I'$  in (25) are even functions of  $x$ , whereas  $\partial_t V$  and  $\partial_t I'$  in (6) are odd.

Given this simple addition, we may directly compare  $D_A$  and  $D_t$  to see which process contributes more to the total phase diffusion rate. For a concrete comparison, we use the well-known soliton model that takes a waveform of  $V = I' = A \operatorname{sech}^2[B(A)(x - v(A)t)]$  with specific expressions for  $B(A)$  and  $v(A)$  found in the Appendix. With this soliton, (29) yields

$$D_A = \left( \frac{\partial v}{\partial A} \right)^2 kT Z_0 \omega_0^2 \tau^2 \frac{r' + g'}{3.8W}. \quad (32)$$

for distributed noise sources. Comparing this with  $D_t$  of (14) that is caused by the same distributed noise sources, we have

$$\frac{D_A}{D_t} \approx 2 \left( \frac{\partial v}{\partial A} \frac{A}{W} \tau \right)^2 \quad (33)$$

Exactly the same relationship holds in the case of lumped noise perturbations, according to (20) and (31) if  $G'_a(t)$  is a constant, which is the case in our experiment. As seen, the ratio depends largely on the velocity-amplitude relation and the life time of amplitude errors.  $D_A$  can be far larger than  $D_t$ , which is the case in our experiment (see Section V).

## V. EXPERIMENT

### A. Oscillator Prototypes

For experimental proof of concept, we designed the sinusoidal standing-wave, linear pulse, and soliton pulse oscillators of Fig. 1(b)–(d) in the lower microwave region. All three oscillators are represented by one schematic in Fig. 6(a). The operation of the active circuit, whose topology is shared by all oscillators, is found in [17]. By adjusting component parameters, the active circuit can amplify small voltages and attenuate large voltages, or vice versa, to produce sinusoidal standing-wave or pulse oscillations. The transmission line in Fig. 6(a) can be linear or nonlinear: the former is for the standing-wave and linear pulse oscillators; the latter is for the soliton pulse oscillator.

The design was implemented on printed circuit boards using discrete components. The standing-wave and linear pulse oscillators were constructed on the same board as one physical structure [see Fig. 6(b)], as they share the same linear line (24 LC sections) and the same active circuit topology. The component parameters in the active circuit are adjusted to switch between standing-wave and linear pulse oscillation. The soliton pulse oscillator on a separate board [see Fig. 6(c)] using a nonlinear line consisting of 24 inductor–varactor sections is an adoption from [17], where we reported the operation of the soliton oscillator.

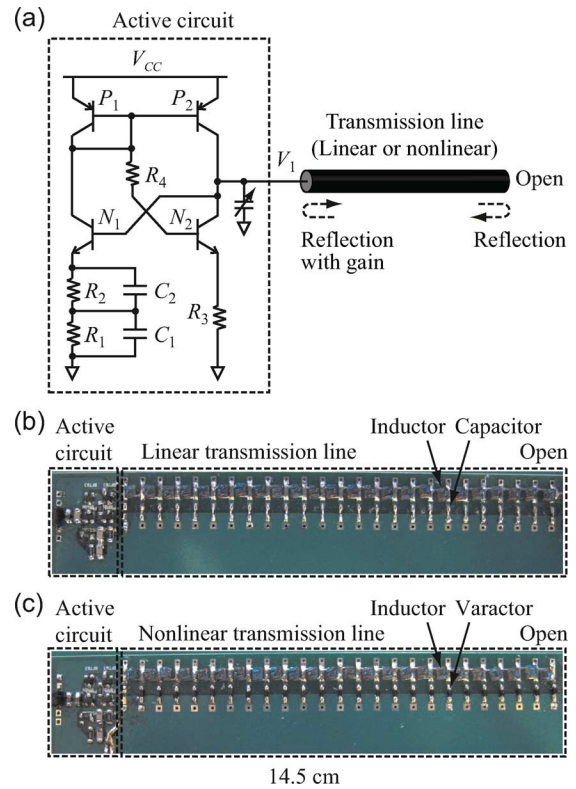


Fig. 6. (a) Schematic of a circuit that can work as a standing-wave, linear pulse, or soliton pulse oscillator, depending on active circuit component parameters and transmission line choice. (b) Implemented circuit that can work as a standing-wave or linear pulse oscillator, depending on active circuit component parameters. (c) Implemented soliton oscillator, adopted from [17].

The oscillators produced desired oscillation waveforms. A 6-V battery was used for a stable power supply. The waveforms were monitored using an Agilent Infiniium 54855A 6-GHz oscilloscope with Agilent 1156A 100-k $\Omega$  active probes. Fig. 7 shows steady-state oscillation waveforms measured at different line positions in each of the three oscillators. Waveform parameters are summarized in Table I. The oscillation frequencies are around 100 MHz for all oscillators. The harmonic contents of the pulse oscillators extend well into the microwave regime.

### B. Phase-Noise Measurement

Fig. 8 shows the phase-noise measurement setup. The transmission line's open end is connected to an Agilent E5052B phase-noise analyzer via an  $L$ -section impedance matching network and a Mini-Circuits ZFL-11AD amplifier. The matching network is to ensure that the line sees a high impedance at what is designed to be an open end so that almost total reflection can occur as intended. The amplifier enhances the weak signal coupled out from the oscillator.

Fig. 9 shows the measured phase noise of the three oscillators. For offset frequencies higher than 10 kHz, the phase-noise data follow closely to an  $f^{-2}$  trend. At lower offset frequencies, the slope is slightly greater than 20 dB/dec, but still closer to 20 dB/dec than 30 dB/dec. This indicates that the noise sources in all oscillators are dominantly white. As predicted, the linear pulse oscillator has a better phase noise than the standing-wave oscillator. The soliton oscillator, despite the soliton pulse's



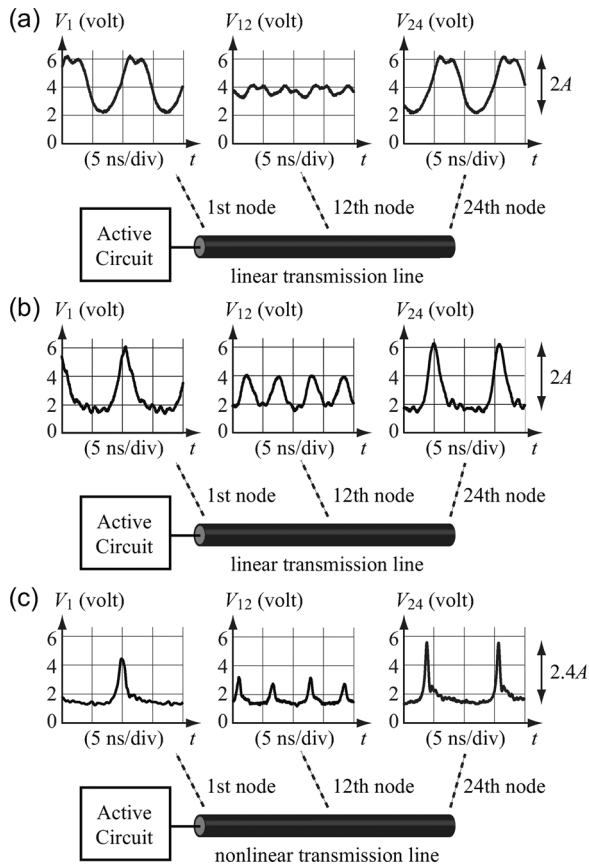


Fig. 7. Measured oscillations. (a) Near-sinusoidal standing-wave oscillator with amplitude  $A = 2$  V. (b) Linear pulse oscillator with pulse amplitude  $A = 2.2$  V and width  $W$  spanning nine and one-half  $LC$  sections. At the open end joint amplitude is  $2A$  due to linear superposition of incident and reflected pulses. (c) Soliton pulse oscillator with  $A \approx 1.8$  V and  $W$  spanning three  $LC$  sections. At the open end joint amplitude is  $2.4A$  due to *nonlinear* superposition [17].

TABLE I  
WAVEFORM PARAMETERS

Oscillator type	Sinusoidal standing	Linear pulse	Soliton pulse
Oscillation frequency (MHz)	95.9	93.3	82.4
Maximum frequency content <sup>a</sup> (MHz)	95.9	373.2	1071.2
Amplitude (volt)	2.0	2.2	1.8 <sup>b</sup>
Pulse Width (section)	-	9.5	3.0

<sup>a</sup>The cutoff is set as the highest harmonics whose power is within  $-20$  dB of the power at the fundamental frequency.

<sup>b</sup>As the soliton pulse propagates along the nonlinear transmission line, it undergoes soliton-shaping and damping processes [Fig. 7(c)] [17] with amplitude,  $A$ , ranging  $1.6 \sim 2.0$  V. An average value is used here for simplicity of analysis.

sharp width, has the worst phase noise due to its amplitude-to-phase-noise conversion, as predicted. Thus, the measurements agree with the core of our theory, which we will further examine quantitatively in Section VI.

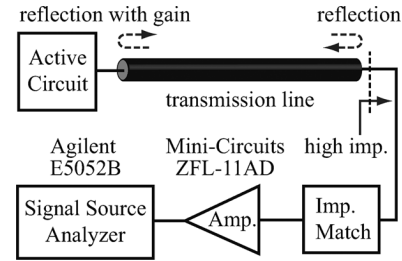


Fig. 8. Phase-noise measurement setup.

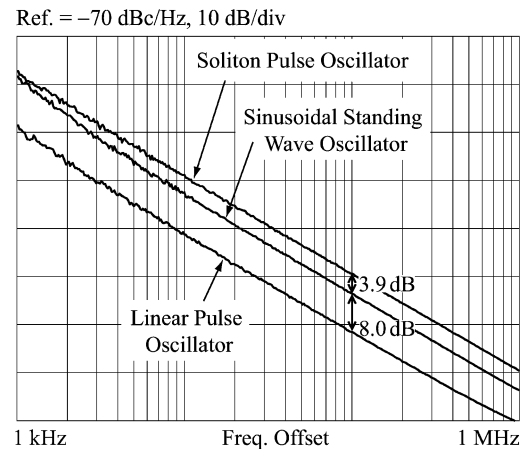


Fig. 9. Measured phase noise for the three oscillators.

## VI. MEASUREMENT-THEORY COMPARISON

We here compare the measured phase noise to phase noise calculated using our theory. For the calculation, we first determine the intensity of the noise sources in the oscillators.

### A. Intensity of Noise Sources

We start with the lumped noise from the active circuit. We observed in all three oscillators that the active circuit remains inactive, except at the rising edge of the voltage signal  $V_1(t)$  at the left end of the line [see Fig. 6(a)] (in a continuous coordinate,  $V_1(t)$  corresponds to  $V(0, t)$ ). The rising edge of  $V_1$  triggers transistors  $N_1$ ,  $P_1$ , and  $P_2$  in Fig. 6(a) so that each pulls a constant current of about 10 mA until  $V_1$  reaches maximum. During this process, energy is injected to provide gain, and also, appreciable noise is injected, as illustrated in Fig. 10.

The intensity of the active noise injected during the rising edge could be measured at dc by biasing the circuit with the same currents (10 mA), as experienced at the rising edge. Such measurement, however, was stymied in our experiment, for 10-mA dc current exceeds the dc breakdown current of transistor  $N_1$ . Even if transistors that could survive the dc current are chosen, the transistors' temperature with the large continuing dc current would be higher than its actual value during the oscillator operation, thus, not necessarily providing a faithful replica of the actual active noise level. We thus chose to carry out the measurement scheme in SPICE simulation. The intensity of the active circuit noise (intensity of  $i_a$  in Fig. 4 multiplied by  $Z_0^2$ ) during the rising edge of  $V_1$  was estimated to be  $4kTZ_0G_a'(t) = 8.5 \times 10^{-17}$  V<sup>2</sup>/Hz for all three oscillators.

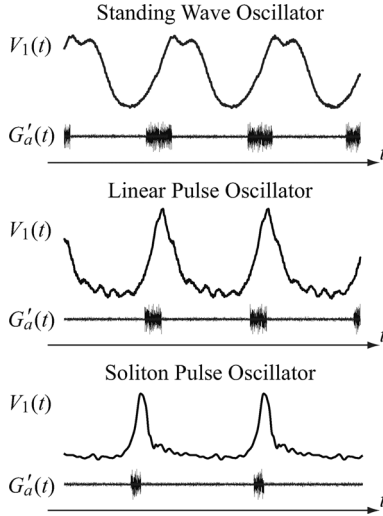


Fig. 10. Time-domain illustration of the lumped noise from the active circuits.

The active noise was negligibly smaller during the rest of  $V_1$  dynamics (Fig. 10).

For the phase-noise calculation, we can effectively reduce this time-varying active noise to a constant noise. Imagine we use  $4kTZ_0G'_a(t) = 8.5 \times 10^{-17} \text{ V}^2/\text{Hz}$  throughout the entire  $V_1$  dynamics in calculating the phase diffusion rate [(19)/(20)], as if it persisted all the time. During the “flat” part of the  $V_1$  waveform, i.e., during the absence of pulse events or transition edges when there is no actual appreciable noise, the fictitious noise does not contribute to (19)/(20), as  $\dot{V}_1(t) = 0$ , thus, its use for the flat duration is justified. During the falling edges, the fictitious noise spuriously contributes the same amount to (19)/(20) as the real noise during the rising edges does, for the oscillation waveforms are almost symmetric about their maxima. Hence, if we use half of the actual noise intensity injected only during the rising edge, i.e.,  $4kTZ_0G'_a = 4.2 \times 10^{-17} \text{ V}^2/\text{Hz}$ , as a constant noise intensity the entire time, it will yield the correct phase diffusion rate. We will use this constant noise in the following analysis for all three oscillators.

The distributed noise in the transmission line is far smaller in our experimental circuits. For both linear and nonlinear lines, the measured  $Q$  is about 100 at the oscillation frequency and measured  $Z_0$  is  $50 \Omega$ , thus, the total noise power of the lossy lines is  $4kTZ_0(\pi/Q) = 2.6 \times 10^{-20} \text{ V}^2/\text{Hz}$ . This is three orders of magnitude smaller than the lumped active noise. In the following calculation of phase noise, we only use the dominant lumped active noise. The oscillation is still distributed while the noise is injected at a fixed point.

### B. Calculated Phase Noise

By plugging the relevant waveform parameters of Table I and the effective constant active noise level into (21) and (22), we find the phase diffusion rate,  $D_t$ , due to direct tangential phase perturbation, for all three oscillators (see Table II). The standing-wave, linear pulse, and soliton pulse oscillators line up in the decreasing order of  $D_t$ , owed to the decreasing waveform width in that order, as explained earlier. In the soliton oscillator, although  $D_t$  is substantially small, we must also consider the phase diffusion rate  $D_A$  due to the indirect phase perturbation

TABLE II  
CALCULATED PHASE DIFFUSION RATES AND PHASE NOISE

Oscillator type	Sinusoidal standing	Linear pulse	Soliton pulse
$D_t$ (direct phase perturbation)(Hz)	0.19	0.079	0.029
$D_A$ (indirect phase perturbation)(Hz)	-	-	0.33
$D_{total} = D_t + D_A$ (Hz)	0.19	0.079	0.36
Phase noise, 100kHz offset (dBc/Hz)	-120.2	-124.0	-117.4

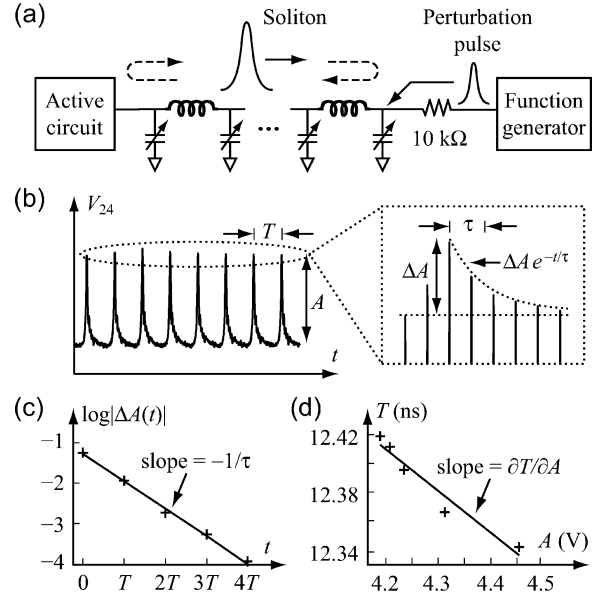


Fig. 11. Measured decay behavior of amplitude perturbation in the soliton oscillator. (a) Measurement setup. (b) Decay behavior after an amplitude perturbation  $\Delta A$ . (c)  $\tau$  extraction. (d)  $\partial T/\partial A$  extraction.

caused by amplitude perturbation and its conversion to phase error. It is shown in Table II as well.

The calculation of  $D_A$  in the soliton oscillator is done as follows. Equation (33) may be rewritten into

$$\frac{D_{A,\text{soliton}}}{D_{t,\text{soliton}}} \approx 2 \left( \frac{\tau A}{T^2} \frac{\partial T}{\partial A} \frac{2d}{W} \right)^2 \quad (34)$$

by using soliton’s round-trip time  $T = 2d/v$  in the nonlinear line. To estimate  $\partial T/\partial A$  and  $\tau$ , we perturb the soliton’s amplitude with a short pulse produced by an Agilent 81150A function generator [see Fig. 11(a)]. From the decaying behavior of the amplitude perturbation, we measure  $A$  and  $T$  of the decaying pulse, as illustrated in Fig. 11(b). From the slopes of  $\log |\Delta A|$  versus  $t$  and  $T$  versus  $A$  [see Fig. 11(c) and (d)], we then obtain  $\tau = (1.50 \pm 0.05)T$  and  $A\partial T/\partial A = -1.20 \pm 0.15 \text{ ns}$ , which are consistent with the standard soliton model (see the Appendix). Plugging these measured values in (34) yields  $D_{A,\text{soliton}} = (11.3 \pm 3.5)D_{t,\text{soliton}} = 0.33 \pm 0.10 \text{ Hz}$ , which enter Table II. In the soliton oscillator, the indirect phase perturbation contributes about ten times more to the total phase noise than the direct phase perturbation. The corresponding calculated phase-noise values for all oscillators at 100-kHz offset are also shown in Table II. The measurement errors in  $\tau$  and

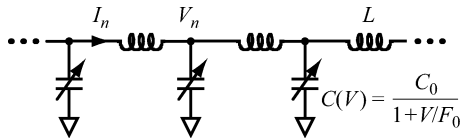


Fig. 12. Standard nonlinear transmission line model.

$A\partial T/\partial A$  give a  $\pm 1.2$ -dB variation in the phase-noise calculation for soliton pulse oscillator.

### C. Measurement-Theory Comparison

Although the calculated and measured phase noise fall within proximity to each other (Fig. 9; Table II), their absolute comparison for each oscillator is not quite meaningful, as the active noise level was only estimated in simulation, because it could not be measured due to the transistor breakdown (see Section VI-A). Since the actual active noise level, albeit not exactly known, is expectedly the same for all three oscillators (see Section VI-A), it would be meaningful to compare the measured and calculated relative phase-noise differences amongst the oscillators. This is because (21) and (22) contain the same active noise term. The relative examination will also facilitate showing the essence of this study, i.e., how oscillation waveforms and their physical nature influence the phase noise. This relative examination we do in the following.

First, when compared to the standing-wave oscillator, the soliton oscillator has a 2.8-dB worse phase noise in calculation (Table II) and a 3.9-dB worse phase noise in measurement (Fig. 9). They are close, consistently explaining that in the soliton oscillator, despite the soliton's sharpness that would yield superb phase noise if only the direct phase perturbation existed, the indirect phase perturbation through amplitude-to-phase error conversion significantly contributes to phase noise, offsetting the benefit of soliton's sharpness. The slight difference between 2.8–3.9 dB may be explained by measurement errors and that our analysis used constant varactor capacitance values for the nonlinear line in the soliton oscillator, while it varies by four times as the varactor voltage changes with the oscillation.

Second, in comparison to the standing-wave oscillator, the linear pulse oscillator has a 3.8-dB better phase noise in calculation (Table II) and an 8.0-dB better phase noise in measurements (Fig. 9). They consistently show the essence, i.e., the phase-noise superiority of the linear pulse oscillator due to its short pulsewidth. The numerical difference may be attributed to that in the actual linear pulse oscillator, the injected noise could have been smaller due to the detailed difference in its operation. Nonetheless, the expected reduction of phase noise for a pulsed waveform is consistently confirmed.

## VII. CONCLUSION

We studied in the time domain how noise perturbs an oscillating electromagnetic wave in distributed oscillators to determine phase noise. In addition to offering an explicit physically intuitive time-domain method to analyze phase noise in

distributed oscillators, this study provides the following few findings.

- 1) While the thermodynamic argument in the Fourier domain fails, our time-domain analysis is suitable in analyzing phase noise in pulse oscillators, where a number of excited modes constituting a pulse are interdependent.
- 2) Phase noise depends on the shape of the electromagnetic wave: the linear pulse oscillator has less phase noise than the sinusoidal standing-wave oscillator, as a sharp electromagnetic pulse has a reduced time period to interact with noise at any given position.
- 3) The soliton oscillator, however, can have a larger phase noise than the standing-wave oscillator despite the soliton's sharpness due to amplitude-to-phase error conversion.

This study highlights a couple of useful design strategies. First, the linear pulse oscillator can achieve superb phase noise if its active circuit, solely responsible for pulse shaping, is designed to produce a very narrow pulse. Second, if the amplitude-to-phase-noise conversion in the soliton oscillator can be mitigated by a proper active circuit design to reduce amplitude error's lifetime, due to the soliton's sharpness, the soliton oscillator can yield superb phase noise.

## APPENDIX

### SOLITON MODEL IN NONLINEAR TRANSMISSION LINE

The nonlinear transmission line is constructed as an inductor–varactor ladder network (Fig. 12). A standard model for the voltage dependency of the varactor capacitance is  $C(V) = C_0/(1 + V/F_0)$  [25]. The corresponding soliton propagating on the line is  $V(n, t) = A \operatorname{sech}^2[B(n - vt)]$  with

$$B(A) = \sinh^{-1} \sqrt{A/F_0}$$

$$v(A) = \frac{\sqrt{A/F_0}}{\sinh^{-1} \sqrt{A/F_0}} \frac{1}{\sqrt{LC_0}}$$

which indicates that a taller soliton pulse has a narrower width and travels faster. The sensitivity of the oscillation period  $T$  to amplitude  $A$  in the soliton oscillator is given by

$$\left| \frac{A}{T} \frac{\partial T}{\partial A} \right| = \left| \frac{A}{v} \frac{\partial v}{\partial A} \right| = \frac{1}{2} \left( 1 - \frac{\sqrt{A/(A + F_0)}}{\sinh^{-1} \sqrt{A/F_0}} \right).$$

Since  $F_0 = 3$  V from the SPICE model and  $A = 1.8$  V,  $W = 1.763/B \approx 2.5$  sections,  $(A/T)|\partial T/\partial A| \approx 0.07$ , and  $D_{A,\text{soliton}}/D_{t,\text{soliton}} \approx 8.4$  (taking  $d = 24$  sections and  $\tau = 1.5T$ ), which are in good agreement with our measurements.

## ACKNOWLEDGMENT

The authors thank N. Sun, Harvard University, Cambridge, MA, for valuable discussions.

## REFERENCES

- [1] M. Lax, "Classical noise. V. Noise in self-sustained oscillators," *Phys. Rev.*, vol. 160, pp. 290–307, Aug. 1967.

- [2] F. X. Kaertner, "Determination of the correlation spectrum of oscillators with low noise," *IEEE Trans. Microw. Theory Tech.*, vol. 37, no. 1, pp. 90–101, Jan. 1989.
- [3] F. X. Kaertner, "Analysis of white and  $f^{-\alpha}$  noise in oscillators," *Int. J. Circuit Theory Appl.*, vol. 18, pp. 485–519, 1990.
- [4] A. Hajimiri and T. H. Lee, "A general theory of phase noise in electrical oscillators," *IEEE J. Solid-State Circuits*, vol. 33, no. 2, pp. 179–194, Feb. 1998.
- [5] A. Demir, A. Mehrotra, and J. Roychowdhury, "Phase noise in oscillators: A unifying theory and numerical methods for characterization," *IEEE Trans. Circuits Syst. I, Fundam. Theory Appl.*, vol. 47, no. 5, pp. 655–674, May 2000.
- [6] A. Demir, "Phase noise and timing jitter in oscillators with colored noise sources," *IEEE Trans. Circuits Syst. I, Fundam. Theory Appl.*, vol. 49, no. 12, pp. 1782–1791, Dec. 2002.
- [7] A. Suarez, S. Sancho, S. Ver Hoeye, and J. Portilla, "Analytical comparison between time- and frequency-domain techniques for phase-noise analysis," *IEEE Trans. Microw. Theory Tech.*, vol. 50, no. 10, pp. 2353–2361, Oct. 2002.
- [8] T. Djurhuus, V. Krozer, J. Vidkjaer, and T. K. Johansen, "Oscillator phase noise: A geometrical approach," *IEEE Trans. Circuits Syst. I, Reg. Papers*, vol. 56, no. 7, pp. 1373–1382, July 2009.
- [9] A. Blaquièrre, *Nonlinear System Analysis*. New York: Academic, 1966.
- [10] K. Kurokawa, *An Introduction to the Theory of Microwave Circuits*. New York: Academic, 1969.
- [11] E. E. Hegazi, J. Rael, and A. Abidi, *The Designer's Guide to High-Purity Oscillators*. Berlin, Germany: Springer, 2004.
- [12] A. Suarez, *Analysis and Design of Autonomous Microwave Circuits*. New York: Wiley, 2009.
- [13] F. O'Mahony, C. P. Yue, M. A. Horowitz, and S. S. Wong, "A 10-GHz global clock distribution using coupled standing-wave oscillators," *IEEE J. Solid-State Circuits*, vol. 38, no. 11, pp. 1813–1820, Nov. 2003.
- [14] W. F. Andress and D. Ham, "Standing wave oscillators utilizing wave-adaptive tapered transmission lines," *IEEE J. Solid-State Circuits*, vol. 40, no. 3, pp. 638–651, Mar. 2005.
- [15] L. A. Glasser and H. A. Haus, "Microwave mode locking at X-band using solid-state devices," *IEEE Trans. Microw. Theory Tech.*, vol. MTT-26, no. 2, pp. 62–69, Feb. 1978.
- [16] D. Ricketts, X. Li, and D. Ham, "Electrical soliton oscillator," *IEEE Trans. Microw. Theory Tech.*, vol. 54, no. 1, pp. 373–382, Jan. 2006.
- [17] O. O. Yildirim, D. Ricketts, and D. Ham, "Reflection soliton oscillator," *IEEE Trans. Microw. Theory Tech.*, vol. 57, no. 10, pp. 2344–2353, Oct. 2009.
- [18] C. J. Madden, R. A. Marsland, M. J. W. Rodwell, D. M. Bloom, and Y. C. Pao, "Hyperabrupt-doped GaAs nonlinear transmission line for picosecond shock-wave generation," *Appl. Phys. Lett.*, vol. 54, no. 11, pp. 1019–1021, Mar. 1989.
- [19] M. Case, M. Kamegawa, R. Y. Yu, M. J. W. Rodwell, and J. Franklin, "Impulse compression using soliton effects in a monolithic GaAs circuit," *Appl. Phys. Lett.*, vol. 58, no. 2, pp. 173–175, Jan. 1991.
- [20] K. S. Giboney, M. J. W. Rodwell, and J. E. Bowers, "Traveling-wave photodetector theory," *IEEE Trans. Microw. Theory Tech.*, vol. 45, no. 8, pp. 1310–1319, Aug. 1997.
- [21] B. Kleveland, C. H. Diaz, D. Vook, L. Madden, T. H. Lee, and S. S. Wong, "Monolithic CMOS distributed amplifier and oscillator," in *IEEE Int. Solid-State Circuits Conf. Tech. Dig.*, Feb. 1999, pp. 70–71.
- [22] D. B. Leeson, "A simple model of feedback oscillator noise spectrum," *Proc. IEEE*, vol. 54, no. 2, pp. 329–330, Feb. 1966.
- [23] J. A. Gubner, *Probability and Random Processes for Electrical and Computer Engineers*. Cambridge, MA: Cambridge Univ. Press, 2006, pp. 453–459.
- [24] M. Lax and W. H. Louisell, "Quantum noise IX: Quantum Fokker-Planck solution for laser noise," *IEEE J. Quantum Electron.*, vol. QE-3, no. 2, pp. 47–58, Feb. 1967.
- [25] M. Toda, *Nonlinear Waves and Solitons*. Norwell, MA: Kluwer, 1989.
- [26] H. A. Haus and Y. Lai, "Quantum theory of soliton squeezing: A linearized approach," *J. Opt. Soc. Amer. B, Opt. Phys.*, vol. 7, no. 3, pp. 386–392, Mar. 1990.



**Xiaofeng Li** was born in Luoyang, China. He received the B.S. degree in electrical engineering from the California Institute of Technology, Pasadena, in 2004, and is currently working toward the Ph.D. degree in electrical engineering from the School of Engineering and Applied Sciences, Harvard University, Cambridge, MA.

His research interests lie in the transformative area of emerging circuits and devices in conjunction with statistical physics, condensed matter physics, and material sciences. His research includes nonlinear electrical soliton oscillators, phase noise of self-sustained electrical oscillators and biological oscillators, and microfluidic stretchable electronics. He is currently conducting an experiment to study gigahertz–terahertz plasmonic waves using 1-D nanoscale devices, and to demonstrate their engineering utility in circuit applications.

Mr. Li was a Gold Medalist at the 29th International Physics Olympiad, Iceland, 1998. He ranked first in the Boston Area Undergraduate Physics Competition in both 2001 and 2002. He was also the recipient of the 2002 California Institute of Technology Henry Ford II Scholar Award, the 2004 Harvard University Peirce Fellowship, and the 2005 Analog Devices Outstanding Student Designer Award.



**O. Ozgur Yildirim** received the B.S. and M.S. degrees in electrical and electronics engineering from Middle East Technical University, Ankara, Turkey, in 2004 and 2006, respectively, and is currently working toward the Ph.D. degree in electrical engineering and applied physics at Harvard University, Cambridge, MA.

In the summers of 2002 and 2003, he was with the Scientific and Research Council of Turkey (TUBITAK), Ankara, Turkey, where he was involved with the development of a dynamic power compensation card and a field-programmable gate array (FPGA) for synchronous dynamic RAM interface. For his Master's research, he was involved with the development of on-chip readout electronics for uncooled microbolometer detector arrays for infrared camera applications. His research interests include ultrafast and RF integrated circuits and devices, soliton and nonlinear waves and their utilization in electronic circuits, and nanoscale and terahertz electronics.

Mr. Yildirim was the recipient of the 2009 Analog Devices Outstanding Student Designer Award.



**Wenjiang Zhu** was born in Lanzhou, China. He received the B.S. degree in chemistry from Peking University, Beijing, China, in 2002, the M.A. degree in chemistry from Princeton University, Princeton, NJ, in 2004, and the Ph.D. degree in chemistry from Harvard University, Cambridge, MA, in 2008. He also received the A.M. degree in statistics from Harvard University, Cambridge, MA, in 2008.

He is currently with JP Morgan, New York, NY. His scientific expertise lies in applying statistical and stochastic methods to a range of dynamical problems

in physics, biology, and finance.



**Donhee Ham** received the B.S. degree (*summa cum laude*) in physics from Seoul National University, Seoul, Korea, in 1996, and the Ph.D. degree in electrical engineering from the California Institute of Technology, Pasadena, in 2002. His doctoral research examined the statistical physics of electrical circuits.

He is currently the Gordon McKay Professor of Applied Physics and Electrical Engineering at Harvard University, Cambridge, MA, where he is with the School of Engineering and Applied Sciences. The intellectual focus of his research laboratory at Harvard University is electronic, electrochemical, and optical biomolecular analysis using silicon integrated circuits and bottom-up nanoscale systems for biotechnology and

medicine; quantum plasmonic circuits using 1-D nanoscale devices; spin-based quantum computing on silicon chips; and RF, analog, and mixed-signal integrated circuits. His research experiences include affiliations with the California Institute of Technology–Massachusetts Institute of Technology (MIT) Laser Interferometer Gravitational Wave Observatory (LIGO), the IBM T. J. Watson Research, and a visiting professorship with POSTECH. He was a coeditor of *CMOS Biotechnology* (2007).

Dr. Ham is a member of the IEEE conference Technical Program Committees including the IEEE International Solid-State Circuits Conference and the IEEE Asian Solid-State Circuits Conference, Advisory Board for the IEEE International Symposium on Circuits and Systems, International Advisory Board for the Institute for Nanodevice and Biosystems, and various U.S., Korea, and Japan industry, government, and academic technical advisory positions on subjects including ultrafast electronics, science and technology at the nanoscale, and convergence of information technology and biotechnology. He was a guest editor

for the IEEE JOURNAL OF SOLID-STATE CIRCUITS. He received the Valedictorian Prize, the Presidential Prize, ranked top first across the Natural Science College of Seoul National University, and also the Physics Gold Medal from Seoul National University. He was the recipient of the Charles Wilts Prize given for the best doctoral dissertation in electrical engineering at the California Institute of Technology. He was the recipient of the IBM Doctoral Fellowship, Caltech Li Ming Scholarship, IBM Faculty Partnership Award, IBM Research Design Challenge Award, Silver Medal in the National Mathematics Olympiad, and Korea Foundation of Advanced Studies Fellowship. He was recognized by *MIT Technology Review* as among the world's top 35 young innovators (TR35) in 2008 for his group's work on CMOS RF nuclear magnetic resonance biomolecular sensor to pursue disease screening and medical diagnostics in a low-cost hand-held platform.